10. Materials and methods are available as supporting material on *Science* Online.
11. U.N. Population Division (UNPD), *World Urbanization Prospects: The 2007 Revision Population Database* (UNPD, New York, 2007); available at http://esa.un.org/unup (accessed September 2007).
12. R. P. Cincotta, J. Wisnewski, R. Engelman, *Nature* **404**, 990 (2000).
13. D. M. Olson *et al.*, *Bioscience* **51**, 933 (2001).
14. A. de Sherbinin, *Oryx* **42**, 26 (2008).
15. UNEP-WCMC, *Prototype Nationally Designated Protected Areas Database* (WCMC/UNEP, Cambridge, 2003); available at www.unep-wcmc.org/protected_areas/data/nat.htm (accessed September 2007).
16. A. N. James, M. J. B. Green, J. R. Paine, *Global Review of Protected Area Budgets and Staff* (WCMC, Cambridge, 1999).
17. A. Balmford, K. J. Gaston, S. Blyth, A. James, V. Kapos, *Proc. Natl. Acad. Sci. U.S.A.* **100**, 1046 (2003).
18. A. James, K. J. Gaston, A. Balmford, *Bioscience* **51**, 43 (2001).
19. GEF, *GEF Biodiversity Strategy in Action* (GEF, Washington, DC, 2006).
20. GEF, *The GEF Project Database* (GEF, Washington, DC, 2008); available at http://gefonline.org/home.cfm (accessed March 2008).
21. W. D. Newmark, J. L. Hough, *Bioscience* **50**, 585 (2000).
22. G. W. Luck, *Biol. Rev. Camb. Philos. Soc.* **82**, 607 (2007).
23. K. K. Karanth, L. M. Curran, J. D. Reuning-Scherer, *Biol. Conserv.* **128**, 147 (2006).
24. J. S. Brashares, P. Arcese, M. K. Sam, *Proc. R. Soc. London B. Biol. Sci.* **268**, 2473 (2001).
25. A. T. Hudak, D. H. K. Fairbanks, B. H. Brockett, *Agric. Ecosyst. Environ.* **101**, 307 (2004).
26. R. DeFries, A. Hansen, A. C. Newton, M. C. Hansen, *Ecol. Appl.* **15**, 19 (2005).
27. E. W. Sanderson *et al.*, *Bioscience* **52**, 891 (2002).
28. R. DeFries, A. Hansen, B. L. Turner, R. Reid, J. G. Liu, *Ecol. Appl.* **17**, 1031 (2007).
29. Overlapping buffers in multiple PAs were combined for analysis, which decreased the sample of 306 PAs to 284 buffer areas. Countries and ecoregions with one park were excluded from statistical analysis of median buffer growth rates, although results did not vary with their inclusion.
30. Supported by NSF OISE-0502340 and the J. S. McDonnell Foundation (G.W.), the Hellman Fund (J.S.B.) and the University of California at Berkeley. We thank A. Balmford, A. Bruner, P. Coppolillo, C. Golden, C. Kremen, R. Kuriyan, J. Scharlemann, A. R. E. Sinclair, C. Stoner, two anonymous reviewers, and the Geospatial Imaging and Informatics Facility (GIIF), Museum of Vertebrate Zoology (MVZ), and Department of Environmental Science, Policy, and Management (ESPM) at the University of California at Berkeley. The authors declare no competing financial interests.

Supporting Online Material

www.sciencemag.org/cgi/content/full/321/5885/123/DC1
Materials and Methods
SOM Text
Figs. S1 to S3
Table S1
References

9 April 2008; accepted 4 June 2008
10.1126/science.1158900

Robust, Tunable Biological Oscillations from Interlinked Positive and Negative Feedback Loops

Tony Yu-Chen Tsai,[1]* Yoon Sup Choi,[1,2]* Wenzhe Ma,[3,4] Joseph R. Pomerening,[5] Chao Tang,[3,4] James E. Ferrell Jr.[1]†

A simple negative feedback loop of interacting genes or proteins has the potential to generate sustained oscillations. However, many biological oscillators also have a positive feedback loop, raising the question of what advantages the extra loop imparts. Through computational studies, we show that it is generally difficult to adjust a negative feedback oscillator's frequency without compromising its amplitude, whereas with positive-plus-negative feedback, one can achieve a widely tunable frequency and near-constant amplitude. This tunability makes the latter design suitable for biological rhythms like heartbeats and cell cycles that need to provide a constant output over a range of frequencies. Positive-plus-negative oscillators also appear to be more robust and easier to evolve, rationalizing why they are found in contexts where an adjustable frequency is unimportant.

The mammalian heart rate is normally established by the sino-atrial node. The node generates constant-amplitude action potentials at a tunable frequency of ~50 to 150 action potentials per minute, depending on the body's oxygen demands. The cell cycle oscillator may also require this combination of an adjustable frequency and invariant amplitude. The period of the cell cycle ranges from about 10 min in rapidly dividing embryos to tens of hours in rapidly dividing somatic cells (and longer in slowly dividing somatic cells), but variations in the amplitude [the peak concentration of active cyclin-dependent kinase-1 (CDK1)] of the oscillations seem neither necessary nor desirable.

Two basic types of circuits have been proposed for biological oscillators: (i) those that contain both positive and negative feedback loops and (ii) those containing only negative feedback (Table 1) (*1*–*6*). Both the sino-atrial node oscillator and the cell cycle oscillator fall into the positive-plus-negative feedback class, suggesting that this design might be better suited for generating oscillations with a tunable frequency and constant amplitude.

We tested this idea through computational studies, beginning with an ordinary differential equation model of CDK1 oscillations in the *Xenopus* embryonic cell cycle (*7*). The model includes a negative feedback loop [active CDK1 brings about its inactivation through the anaphase-promoting complex (APC)] and a pair of positive feedback loops (active CDK1 activates its activator Cdc25 and inactivates its inhibitor Wee1) (Fig. 1A). We specified the strength of the positive feedback through a parameter r, the ratio of the activities of Cdc25 and Wee1 in interphase versus M phase. Because the rate of cyclin synthesis determines the frequency of CDK1 oscillations in *Xenopus* embryos (*7*, *8*), we varied the cyclin synthesis rate constant k_{synth} in the model and determined how the amplitude and frequency of the oscillations were affected by this variation.

In the negative feedback–only version of the model ($r = 1$ in Fig. 1, B and C), a relatively small range of k_{synth} values yielded oscillations. Plotting the amplitude and frequency of the oscillations on a log-log plot yielded a tight, inverted U-shaped curve (Fig. 1B). The range of frequencies over which the oscillator functioned was small (1.7-fold), and even within this range, the frequency could not be adjusted without compromising the amplitude substantially.

Adding positive feedback markedly changed the amplitude/frequency relation (Fig. 1, B and C). At a biologically realistic feedback strength of $r = 10$ (*9*–*11*), the oscillator functioned over a 4900-fold range of frequencies (Fig. 1B, green points). Over much of this range, the frequency of the oscillator was linearly proportional to k_{synth}, and the amplitude was approximately constant (Fig. 1, B and C). Thus, positive feedback provided a highly tunable frequency and robust amplitude.

Something other than the cyclin synthesis rate may tune the frequencies of some cell cycles. We therefore asked whether the negative feedback–only oscillator might operate over a wider range of frequencies if one of the model's other 20 parameters were varied. This was not the case; invariably, the oscillator operated over only a narrow frequency range. Of course if all of the rate constants were multiplied by the same factor (equivalent to scaling the units of time), the oscillator's frequency could be varied without changing the amplitude. However, this type of coordinated regulation is not relevant to any of the biological oscillators that we are familiar with (Table 1).

[1]Department of Chemical and Systems Biology, Stanford University School of Medicine, Stanford, CA 94305–5174, USA. [2]School of Interdisciplinary Bioscience and Bioengineering, Pohang University of Science and Technology, Pohang, 790-784, Republic of Korea. [3]Center for Theoretical Biology, Peking University, Beijing, 100871, China. [4]California Institute for Quantitative Biosciences, University of California, San Francisco, CA 94143–2540, USA. [5]Department of Biology, Indiana University, Bloomington, IN 47405, USA.

*These authors contributed equally to this work.
†To whom correspondence should be addressed. E-mail: james.ferrell@stanford.edu

Both the tunable frequency and constant amplitude of the positive-plus-negative feedback cell cycle model arise because the system behaves like a relaxation oscillator (*12*–*15*). Relaxation oscillators are built on a hysteretic switch, and experimental studies have shown that in *Xenopus* extracts the response of the CDK1/Cdc25/Wee1/Myt1 positive feedback loop is hysteretic, resembling that shown in Fig. 2A (*16*, *17*).

To see how relaxation oscillations can arise from a hysteretic switch and to see why this permits a tunable period and constant amplitude, assume that a cell cycle begins with no cyclin B and no active CDK1 and that cyclin B synthesis is slow relative to the phosphorylation and dephosphorylation reactions that allow the hysteretic switch to approach its steady state (Fig. 2A). As cyclin B accumulates, the system moves up the lower branch of the stimulus/response curve, and the CDK1 activity slowly rises (Fig. 2, A and B, segments 0 and 1). Ultimately, the branch terminates and the system switches ("relaxes") to the other branch (Fig. 2, A and B, segment 2).

Now assume that at this higher, mitotic level of CDK1 activity, the APC is turned on and the cyclin B concentration begins to fall slowly. The system progresses down the upper branch of the stimulus/response curve (Fig. 2, A and B, segment 3) until the branch terminates and the system switches to the lower branch (Fig. 2, A and B, segment 4). The APC turns back off, cyclin B reaccumulates, and the cycle starts over. Thus, oscillations in this system essentially represent a walk around the hysteretic steady-state stimulus/response loop. The frequency of the oscillator is determined by how rapid the walk is, and the amplitude (the height of the loop) is constant.

In reality, the rate of cyclin B destruction by the APC is not slow compared with the phosphorylation and dephosphorylation reactions (*7*). This fact is incorporated into the cell cycle model examined here, and it makes the orbits of the oscillator overshoot the hysteretic loop (Fig. 2C). Nevertheless, the model still behaves much like a relaxation oscillator, especially at low k_{synth} values (Fig. 2, C and D).

To test the generality of the idea that positive feedback enables an oscillator to have a tunable frequency and constant amplitude, we examined several other oscillator models, including five negative feedback–only models: (i) the Goodwin oscillator, a well-studied model relevant to circadian oscillations (*18*, *19*); (ii) the Repressilator, a transcriptional triple-negative feedback loop constructed in *Escherichia coli* (*20*); (iii) the "Pentilator," a Repressilator with five (rather than three) repressors; (iv) the Metabolator (*21*), a synthetic metabolic oscillator; and (v) the Frzilator, a model of the control of gliding motions in myxobacteria (*22*). In four of the cases (Goodwin, Repressilator, Pentilator, and Metabolator), the amplitude/frequency curves were inverted U-shaped curves similar to that seen for the negative feedback–only cell cycle model (Figs. 1B and 3A). In the case of the

Table 1. Positive feedback loops in biological oscillators.

Oscillator	Period	Positive feedback	Refs.
Sino-atrial pacemaker	~1 s	Depolarization → Na^+ channel activation → depolarization	(*29*)
Calcium spikes	~100 s	Cytoplasmic Ca^{2+} → PLC → IP_3 → cytoplasmic Ca^{2+} Cytoplasmic Ca^{2+} → IP_3R → cytoplasmic Ca^{2+} Cytoplasmic Ca^{2+} → IP_3R -| ER Ca^{2+} -| SOC → cytoplasmic Ca^{2+}	(*25*, *30*, *31*)
Myxobacterial gliding	~10 min	None known	(*22*)
Animal cell cycle (*Xenopus laevis* embryos)	~30 min	Cdk1 → Cdc25 → Cdk1 Cdk1 -| Wee1 -| Cdk1 Cdk1 -| Myt1 -| Cdk1	(*32*, *33*)
Somitogenesis	~30 min	DeltaC → Notch → DeltaC	(*34*)
Yeast cell cycle (*S. cerevisiae*)	~2 hours	CLN1,2 transcription → CDK1 → CLN1,2 transcription CDK1 -| Sic1 -| CDK1 CDK1 -| Cdh1 -| CDK1	(*6*, *35*–*39*)
NF-κB responses	~100 min	None known	(*40*, *41*)
p53 responses	~100 min	p53 → PTEN -| Akt → Mdm2 -| p53 p53 → p21 -| Cdk2 -| Rb -| Mdm2 -| p53	(*42*, *43*)
Animal cell cycle (somatic cells)	~24 hours	CDK2 -| Rb -| E2F → CDK2 Cdk1 → Cdc25 → Cdk1 Cdk1 -| Wee1 -| Cdk1 Cdk1 -| Myt1 -| Cdk1	(*44*)
Circadian rhythm (mammals)	~24 hours	BMAL1 → Rora → BMAL1	(*45*)
Circadian rhythm (*Drosophila*)	~24 hours	CLK → PDP1 → CLK	(*45*)
Circadian rhythm (fungi)	~24 hours	FRQ → WC-1 → FRQ	(*46*)
Circadian rhythm (cyanobacteria)	~24 hours	KaiC-SP -| KaiA -| KaiC-SP	(*26*)

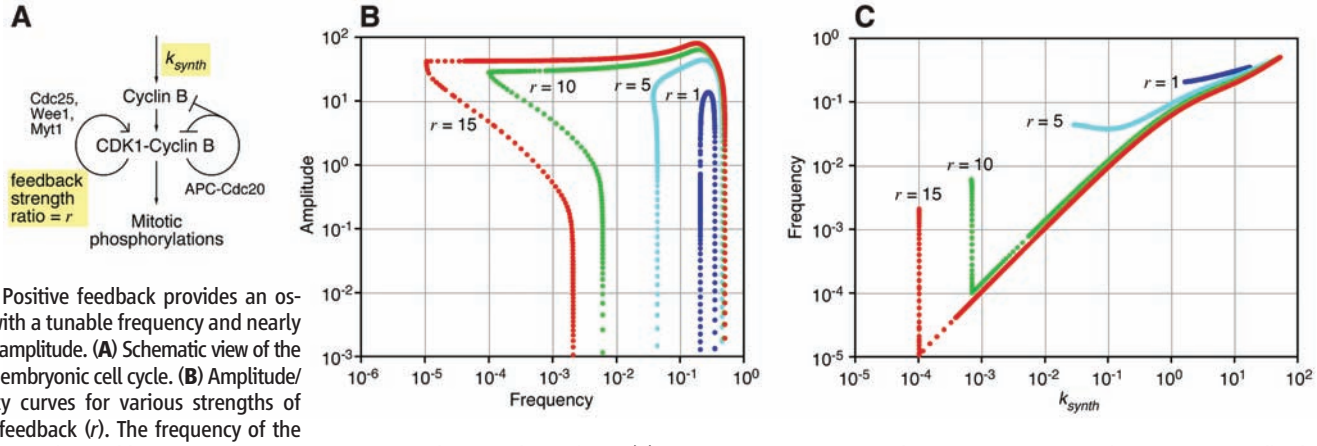

Fig. 1. Positive feedback provides an oscillator with a tunable frequency and nearly constant amplitude. (**A**) Schematic view of the *Xenopus* embryonic cell cycle. (**B**) Amplitude/frequency curves for various strengths of positive feedback (*r*). The frequency of the oscillator was changed by varying the rate constant for cyclin B synthesis, k_{synth}. (**C**) Frequency as a function of k_{synth} for various strengths of positive feedback.

Frzilator, the legs of the curve were truncated; the oscillator had a nonzero minimal amplitude (Fig. 3A). For all five of the negative feedback–only models, the oscillators functioned over only a narrow range of frequencies (Fig. 3A).

We also examined four positive-plus-negative feedback oscillators: (i) the van der Pol oscillator, inspired by studies of vacuum tubes (*12*); (ii) the Fitzhugh-Nagumo model of propagating action potentials (*23*, *24*); (iii) the Meyer-Stryer model of calcium oscillations (*25*); and (iv) a model of circadian oscillations in the cyanobacterial KaiA/B/C system (*26*–*28*). In each case, we obtained a flat, wide amplitude/frequency curve (Fig. 3B). Thus, a tunable frequency plus constant amplitude can be obtained from many different positive-plus-negative feedback models; this feature is not peculiar to one particular topology or parameterization.

These findings rationalize why the positive-plus-negative feedback design might have been selected through evolution in cases where a tunable frequency and constant amplitude are important, such as heartbeats and cell cycles. However, it is not clear that an adjustable frequency would be advantageous for circadian oscillations, because frequency is fixed at one cycle per day. Nevertheless, the cyanobacterial circadian oscillator appears to rely on positive feedback (*26*), and positive feedback loops have been postulated for other circadian oscillators as well (Table 1). This raises the question of whether the positive-plus-negative feedback design might offer additional advantages.

One possibility is that the positive-plus-negative feedback design permits oscillations over a wider range of enzyme concentrations and kinetic constant values, making the oscillator easier to evolve and more robust to variations in its imperfect components. We tested this idea through a Monte Carlo approach. We formulated three simple oscillator models: (i) a three-variable triple negative feedback loop with no additional feedback (Fig. 4A), (ii) one with added positive feedback (Fig. 4B), or (iii) one with added negative feedback (Fig. 4C). We generated random parameter sets for the models and then for each set determined whether the model produced limit cycle oscillations. We continued generating parameter sets until we had amassed 500 that gave oscillations.

For the negative feedback–only model, 500 out of 138,785 parameter sets (0.36%) yielded oscillations (Fig. 4D). For the positive-plus-negative feedback model, oscillatory parameter sets were found at a higher rate: 500 out of 23,848 parameter sets (2.1%) if we assumed weak positive feedback and 500 out of 9854 sets (5.1%) for strong positive feedback (Fig. 4D). The negative-plus-negative feedback model yielded oscillations at a lower rate than even the negative feedback–only model: 500 out of 264,672 parameter sets (0.19%) for the weaker feedback strength and 500 out of 583,263 (0.086%) for the stronger feedback. This is probably because the short negative feedback loop stabilizes the output of *A*, making it difficult for changes in *C*'s activity to be propagated onward. Thus, the positive-plus-negative feedback design was substantially more robust, by this measure, than either the negative feedback–only model or the negative-plus-negative feedback model.

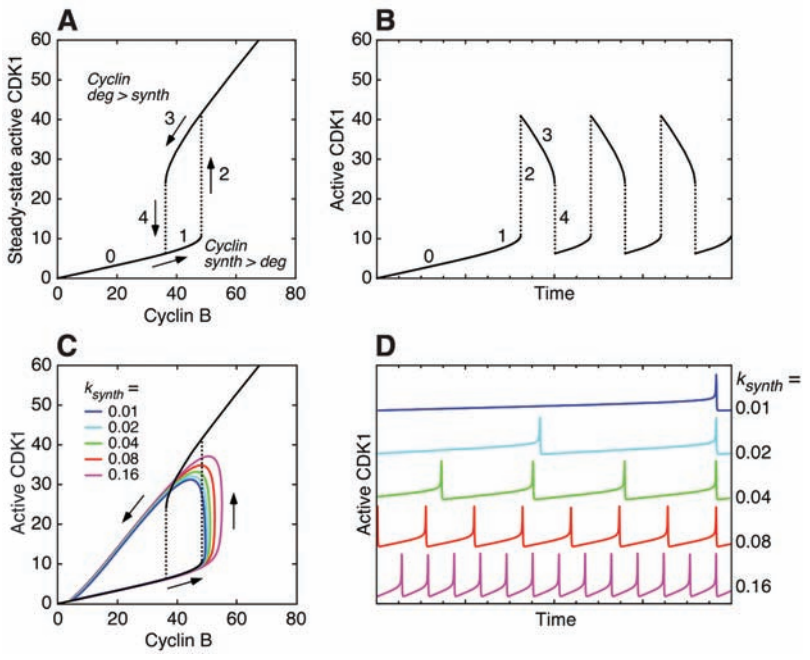

Fig. 2. From a hysteretic switch to a relaxation oscillator. (**A**) Hysteretic steady-state response of CDK1 to cyclin B, on the basis of previous experimental studies (*16*, *17*). (**B**) CDK1 activation and inactivation in the limit of slow cyclin B synthesis and degradation. (**C** and **D**) Cell cycle model run with biologically realistic parameters, showing a looser relation between the oscillations and the hysteretic steady-state response.

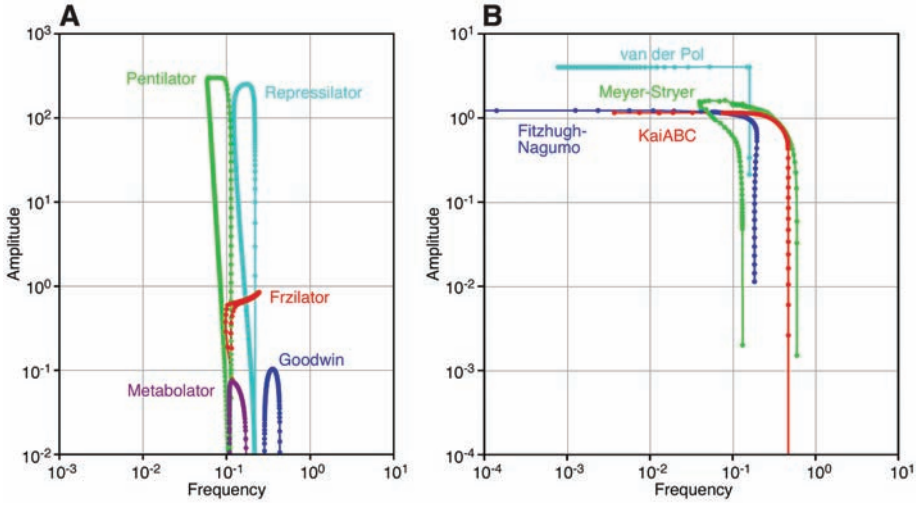

Fig. 3. Amplitude/frequency curves for various legacy oscillators. (**A**) Negative feedback–only models. (**B**) Positive-plus-negative feedback models.

The random parameter sets also provided a further test of the hypothesis that the positive-plus-negative design allows for a tunable frequency. For each oscillatory set, we varied one parameter (k_3) and calculated amplitude/frequency curves and operational frequency ranges. For the negative feedback–only and the negative-plus-negative feedback models, all of the oscillatory parameter sets yielded narrow, inverted U-shaped amplitude/frequency curves with small operational frequency ranges (Fig. 4, E and F, and fig. S1). In contrast, many of the amplitude/frequency curves for the positive-plus-negative feedback model were flat and wide, with large operational frequency ranges (Fig. 4, E and F). Thus, the positive-plus-negative design provided the possibility of a tunable frequency and near-constant amplitude.

The frequent presence of positive feedback loops in natural biological oscillators suggests

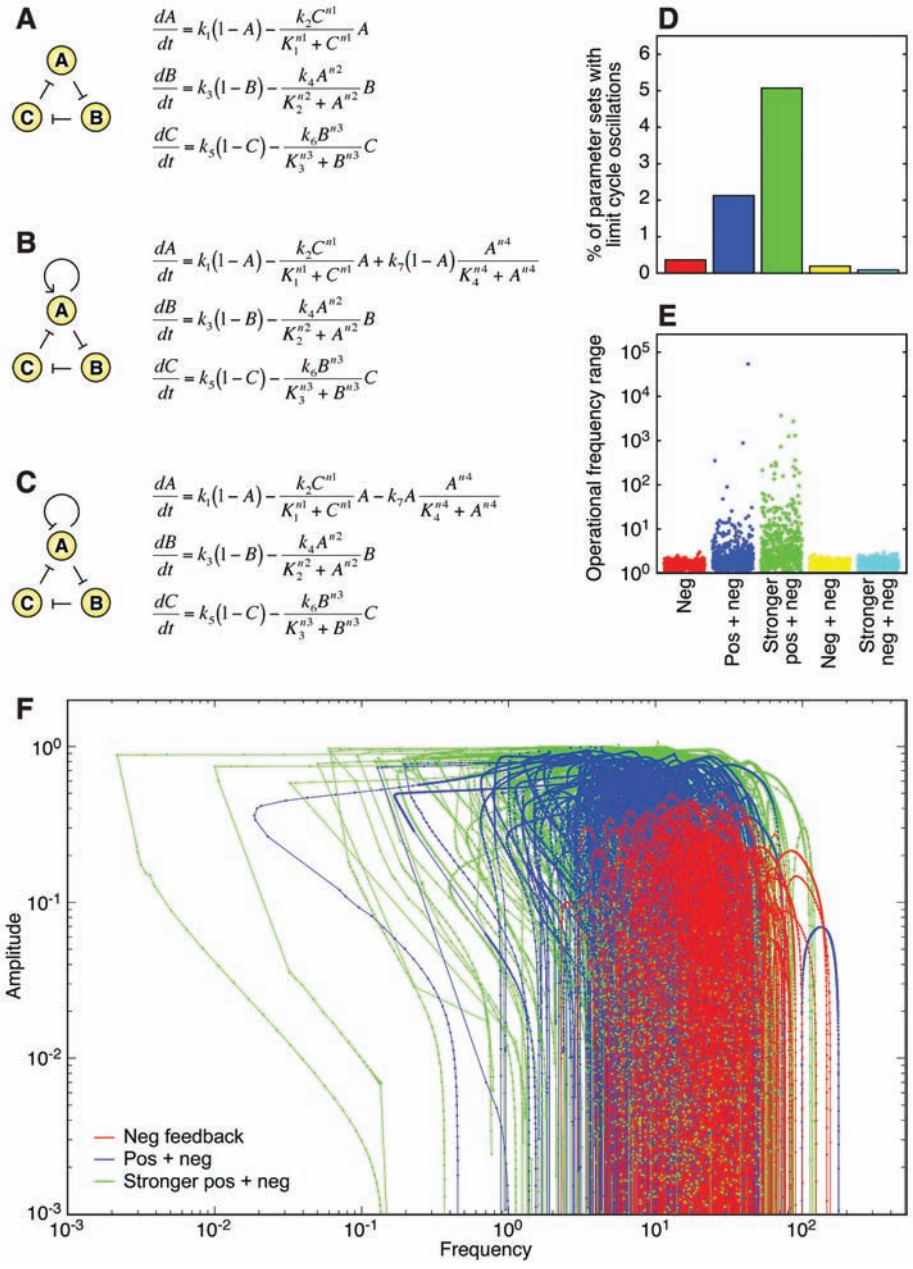

Fig. 4. Randomly parameterized oscillator models. (**A**) Negative feedback–only. *A*, *B*, and *C*, the fractions of proteins A, B, and C that are active; *K*, median effective concentration values of the Hill functions; *n*, Hill coefficients; *k*, rate constants. (**B**) Positive-plus-negative feedback. (**C**) Negative-plus-negative feedback. (**D**) Percentage of parameter sets that yielded limit cycle oscillations. For the positive-plus-negative and negative-plus-negative models, we looked at two ranges of feedback strengths: (i) k_7 = 0 to 100 (weak) and (ii) k_7 = 500 to 600 (strong). (**E**) Operational frequency ranges for the oscillators. Each point represents $freq_{max}/freq_{min}$ for one of the 2500 parameter sets that produced oscillations, with k_3 as the bifurcation parameter. Mean operational frequency ranges were 1.6, 370, 63, 1.6, and 1.6. Medians were 1.6, 2.2, 3.3, 1.6, and 1.6. (**F**) Amplitude/frequency curves for the randomly parameterized models. We show 300 out of 500 curves for the negative feedback–only model (red) and the positive-plus-negative feedback model with weak (blue) or strong (green) positive feedback. Curves for the negative-plus-negative feedback model are shown in fig. S1.

that this type of circuit possesses some performance advantages over simple negative feedback loops. The present work demonstrates two such advantages: (i) the ability to tune the oscillator's frequency without changing its amplitude and (ii) a greater robustness and reliability.

References and Notes

1. C. D. Thron, *Biophys. Chem.* **57**, 239 (1996).
2. A. Goldbeter *et al.*, *Chaos* **11**, 247 (2001).
3. J. J. Tyson, K. C. Chen, B. Novak, *Curr. Opin. Cell Biol.* **15**, 221 (2003).
4. P. Smolen, D. A. Baxter, J. H. Byrne, *Am. J. Physiol.* **274**, C531 (1998).
5. A. Goldbeter, *Nature* **420**, 238 (2002).
6. F. R. Cross, *Dev. Cell* **4**, 741 (2003).
7. J. R. Pomerening, S. Y. Kim, J. E. Ferrell Jr., *Cell* **122**, 565 (2005).
8. R. S. Hartley, R. E. Rempel, J. L. Maller, *Dev. Biol.* **173**, 408 (1996).
9. A. Kumagai, W. G. Dunphy, *Cell* **70**, 139 (1992).
10. P. R. Mueller, T. R. Coleman, W. G. Dunphy, *Mol. Biol. Cell* **6**, 119 (1995).
11. S. Y. Kim, E. J. Song, K. J. Lee, J. E. Ferrell Jr., *Mol. Cell. Biol.* **25**, 10580 (2005).
12. B. van der Pol, J. van der Mark, *Philos. Mag.* **6** (suppl.), 763 (1928).
13. H. S. Hahn, A. Nitzan, P. Ortoleva, J. Ross, *Proc. Natl. Acad. Sci. U.S.A.* **71**, 4067 (1974).
14. C. R. Nave, *Hyperphysics* (1995), (http://hyperphysics.phy-astr.gsu.edu/Hbase/electronic/relaxo.html).
15. S. H. Strogatz, *Nonlinear Dynamics and Chaos: With Applications to Physics, Biology, Chemistry, and Engineering* (Westview, Cambridge MA, 1994).
16. W. Sha *et al.*, *Proc. Natl. Acad. Sci. U.S.A.* **100**, 975 (2003).
17. J. R. Pomerening, E. D. Sontag, J. E. Ferrell Jr., *Nat. Cell Biol.* **5**, 346 (2003).
18. B. C. Goodwin, Ed. *Oscillatory Behavior in Enzymatic Control Processes*, vol. 3 (Permagon, Oxford, 1965), pp. 425–438.
19. P. Ruoff, S. Mohsenzadeh, L. Rensing, *Naturwissenschaften* **83**, 514 (1996).
20. M. B. Elowitz, S. Leibler, *Nature* **403**, 335 (2000).
21. E. Fung *et al.*, *Nature* **435**, 118 (2005).
22. O. A. Igoshin, A. Goldbeter, D. Kaiser, G. Oster, *Proc. Natl. Acad. Sci. U.S.A.* **101**, 15760 (2004).
23. R. FitzHugh, *Biophys. J.* **1**, 445 (1961).
24. J. Nagumo, S. Arimoto, S. Yoshizawa, *Proc. IRE* **50**, 2061 (1964).
25. T. Meyer, L. Stryer, *Proc. Natl. Acad. Sci. U.S.A.* **85**, 5051 (1988).
26. M. J. Rust, J. S. Markson, W. S. Lane, D. S. Fisher, E. K. O'Shea, *Science* **318**, 809 (2007); published online 4 October 2007, 10.1126/science.1148596.
27. M. Nakajima *et al.*, *Science* **308**, 414 (2005).
28. T. Nishiwaki *et al.*, *EMBO J.* **26**, 4029 (2007).
29. A. L. Hodgkin, A. F. Huxley, *J. Physiol.* **117**, 500 (1952).
30. R. S. Lewis, *Annu. Rev. Immunol.* **19**, 497 (2001).
31. M. J. Berridge, *Novartis Found. Symp.* **239**, 52 (2001).
32. B. Novak, J. J. Tyson, *J. Cell Sci.* **106**, 1153 (1993).
33. J. J. Tyson, B. Novak, *J. Theor. Biol.* **210**, 249 (2001).
34. A. Mara, S. A. Holley, *Trends Cell Biol.* **17**, 593 (2007).
35. K. Levine, A. H. Tinkelenberg, F. Cross, *Prog. Cell Cycle Res.* **1**, 101 (1995).
36. J. M. Bean, E. D. Siggia, F. R. Cross, *Mol. Cell* **21**, 3 (2006).
37. D. Stuart, C. Wittenberg, *Genes Dev.* **9**, 2780 (1995).
38. L. Dirick, K. Nasmyth, *Nature* **351**, 754 (1991).
39. K. C. Chen *et al.*, *Mol. Biol. Cell* **15**, 3841 (2004).
40. A. Hoffmann, A. Levchenko, M. L. Scott, D. Baltimore, *Science* **298**, 1241 (2002).
41. D. E. Nelson *et al.*, *Science* **306**, 704 (2004).
42. R. Lev Bar-Or *et al.*, *Proc. Natl. Acad. Sci. U.S.A.* **97**, 11250 (2000).
43. G. Lahav *et al.*, *Nat. Genet.* **36**, 147 (2004).
44. L. A. Buttitta, B. A. Edgar, *Curr. Opin. Cell Biol.* **19**, 697 (2007).
45. M. Gallego, D. M. Virshup, *Nat. Rev. Mol. Cell Biol.* **8**, 139 (2007).
46. K. Lee, J. J. Loros, J. C. Dunlap, *Science* **289**, 107 (2000).

47. We thank E. Sontag, A. Millar, and B. Novak for helpful discussions; J. Hasty for communicating unpublished results; and J. Ubersax and G. Anderson for comments on the manuscript. This work was supported by grants from NIH (GM61726 and GM77544), by the Li Foundation, and by a Korea Science and Engineering Foundation grant from the Korean government (No. R15-2004-033-05002-0).

Supporting Online Material

www.sciencemag.org/cgi/content/full/321/5885/126/DC1
SOM Text
Fig. S1
Table S1
References

25 February 2008; accepted 9 June 2008
10.1126/science.1156951

Supporting Online Material

Robust, tunable biological oscillations from interlinked positive and negative feedback loops

Tony Yu-Chen Tsai, Yoon Sup Choi, Wenzhe Ma, Joseph R. Pomerening, Chao Tang, and James E. Ferrell, Jr.

Computational modeling

For each ordinary differential equation (ODE) model analyzed, we solved the differential equations numerically using a Runge-Kutta method. To construct amplitude vs. frequency curves, we first chose a bifurcation parameter and then identified the range of the parameter over which the system exhibited limit cycle oscillations by locating the Hopf bifurcations at which oscillations were born and extinguished. We then used an iterative algorithm to march along the chosen parameter between the two bifurcations. For each set of parameters we calculated the limit cycle solution of the system, keeping track of the amplitude and frequency of the limit cycle solution. We made use of Mathematica (Wolfram Research, Inc.) and MatCONT (*S1*), a public toolbox for bifurcation analysis in Matlab (The MathWorks Inc.), for these computations.

Below we describe the ODE models, parameter sets, and bifurcation parameters we examined.

1. Negative feedback and positive-plus-negative feedback cell cycle oscillators. This is a nine ODE model of the embryonic mitotic oscillator in *Xenopus laevi*s (*S2*). Depending upon parameter choice, the model can function as a negative feedback circuit or as a positive-plus-negative feedback circuit. Parameters were chosen so that at a realistic feedback strength of r=10, the model would reproduce the experimental curves for the steady-state activity of CDK1 as a function of constant cyclin concentration, and for the time course of CDK1 activation when driven by a constant rate of cyclin synthesis (*S2, S3*).

To make it easier to distinguish between complexes (e.g. CDK1-cyclin) and products of individual species (e.g. CDK1 × cyclin), for this model we have written all time-dependent species as explicit functions of time. Thus, *cdk1cyclin*[*t*] represents the concentration of the CDK1-cyclin complex, whereas *cdk1*[*t*]*cyclin*[*t*] represents the product of the free CDK1 and cyclin concentrations.

ODEs:

$$\frac{dcyclin[t]}{dt} = k_{synth} - k_{dest} apc_{act}[t] cyclin[t] -$$
$$k_a\left(cdk1_{tot} - cdk1cyclin[t] - cdk1cyclinyp[t] - cdk1cyclinyptp[t] - cdk1cyclintp[t]\right)cyclin[t] +$$
$$k_d cdk1cyclin[t]$$

$$\frac{dcdk1cyclin[t]}{dt} =$$
$$k_a\left(cdk1_{tot} - cdk1cyclin[t] - cdk1cyclinyp[t] - cdk1cyclinyptp[t] - cdk1cyclintp[t]\right)cyclin[t] -$$
$$k_d cdk1cyclin[t] - k_{dest} apc_{act}[t] cdk1cyclin[t] - k_{wee1} wee1_{act}[t] cdk1cyclin[t] -$$
$$k_{wee1basal}\left(wee1_{tot} - wee1_{act}[t]\right)cdk1cyclin[t] + k_{cdc25} cdc25_{act}[t] cdk1cyclinyp[t] +$$
$$k_{cdc25basal}\left(cdc25_{tot} - cdc25_{act}[t]\right)cdk1cyclinyp[t]$$

$$\frac{dcdk1cyclinyp[t]}{dt} = k_{wee1} wee1_{act}[t] cdk1cyclin[t] + k_{wee1basal}\left(wee1_{tot} - wee1_{act}[t]\right)cdk1cyclin[t] -$$
$$k_{cdc25} cdc25_{act}[t] cdk1cyclinyp[t] - k_{cdc25basal}\left(cdc25_{tot} - cdc25_{act}[t]\right)cdk1cyclinyp[t] -$$
$$k_{cak} cdk1cyclinyp[t] + k_{pp2c} cdk1cyclinyptp[t] - k_{dest} apc_{act}[t] cdk1cyclinyp[t]$$

$$\frac{dcdk1cyclinyptp[t]}{dt} = k_{cak} cdk1cyclinyp[t] - k_{pp2c} cdk1cyclinyptp[t] -$$
$$k_{cdc25} cdc25_{act}[t] cdk1cyclinyptp[t] - k_{cdc25basal}\left(cdc25_{tot} - cdc25_{act}[t]\right)cdk1cyclinyptp[t] +$$
$$k_{wee1} wee1_{act}[t] cdk1cyclintp[t] + k_{wee1basal}\left(wee1_{tot} - wee1_{act}[t]\right)cdk1cyclintp[t] -$$
$$k_{dest} apc_{act}[t] cdk1cyclinyptp[t]$$

$$\frac{dcdk1cylintp[t]}{dt} = k_{cdc25} cdc25_{act}[t] cdk1cyclinyptp[t] +$$
$$k_{cdc25basal}\left(cdc25_{tot} - cdc25_{act}[t]\right)cdk1cyclinyptp[t] - k_{wee1} wee1_{act}[t] cdk1cyclintp[t] -$$
$$k_{wee1basal}\left(wee1_{tot} - wee1_{act}[t]\right)cdk1cyclintp[t] - k_{dest} apc_{act}[t] cdk1cyclintp[t]$$

$$\frac{dcdc25_{act}[t]}{dt} = k_{cdc25on}\left(\frac{cdk1cyclintp[t]^{ncdc25}}{ec50_{cdc25}^{ncdc25} + cdk1cyclintp[t]^{ncdc25}}\right)\left(cdc25_{tot} - cdc25_{act}[t]\right) -$$
$$k_{cdc25off} cdc25_{act}[t]$$

$$\frac{dwee1_{act}[t]}{dt} = -k_{wee1off}\left(\frac{cdk1cyclintp[t]^{nwee1}}{ec50_{wee1}^{nwee1} + cdk1cyclintp[t]^{nwee1}}\right)wee1_{act}[t] + k_{wee1on}\left(wee1_{tot} - wee1_{act}[t]\right)$$

$$\frac{dplx1}{dt} = k_{plx1on}\left(\frac{cdk1cyclintp[t]^{nplx1}}{ec50_{plx1}^{nplx1} + cdk1cyclintp[t]^{nplx1}}\right)\left(plx1_{tot} - plx1_{act}[t]\right) - k_{plx1off} plx1_{act}[t]$$

$$\frac{dapc_{act}[t]}{dt} = k_{apcon}\left(\frac{plx1_{act}[t]^{napc}}{ec50_{plx1}^{napc} + plx1_{act}[t]^{napc}}\right)\left(apc_{tot} - apc_{act}[t]\right) - k_{apcoff} apc_{act}[t]$$

Initial conditions:

$$cyclin[0] = 0$$

$$cdk1cyclin[0] = 0$$

$$cdk1cyclinyp[0] = 0$$

$cdk1cyclinyptp[0] = 0$

$cdk1cyclintp[0] = 0$

$cdc25_{act}[0] = 0$

$wee1_{act}[0] = wee1_{tot}$

$plx_{act}[0] = 0$

$apc_{act}[0] = 0$

Parameters:

$k_{dest} = 0.01$

$k_a = 0.1$

$k_d = 0.001$

$k_{wee1} = 0.05$

$k_{wee1basal} = k_{wee1} / r$

$k_{cdc25} = 0.1$

$k_{cdc25basal} = k_{cdc25} / r$

$cdc2_{tot} = 230$

$cdc25_{tot} = 15$

$wee1_{tot} = 15$

$apc_{tot} = 50$

$plx1_{tot} = 50$

$nwee1 = 4$

$ncdc25 = 4$

$napc = 4$

$nplx1 = 4$

$ec50_{plx1} = 40$

$ec50_{wee1} = 40$

$ec50_{cdc25} = 40$

$ec50_{apc} = 40$

$k_{cdc25on} = 1.75$

$k_{cdc25off} = 0.2$

$k_{apcon} = 1$

$k_{apcoff} = 0.15$

$k_{plx1on} = 1$

$k_{plxoff} = 0.15$

$k_{wee1on} = 0.2$

$k_{wee1off} = 1.75$

$k_{cak} = 0.8$

$k_{pp2c} = 0.008$

For the negative feedback model, we took $r = 1$, which is equivalent to assuming that the activities of Wee1 and Cdc25 are not affected by the activity of CDK1. For the positive-plus-negative feedback model, we took $r = 5$, 10, or 15 to compare the effects of different feedback strengths. In all cases, the oscillations were found to be born and extinguished through supercritical Hopf bifurcations. Thus a change in the type of bifurcation was not responsible for the change in the shape of the amplitude vs. frequency curves that positive feedback produced.

The following five models are negative-feedback-only oscillators:

2. Repressilator. Elowitz and Leibler used a six variable ODE model to guide their construction of the Repressilator, an artificial negative feedback oscillator, in *E. coli* (*S4*). The model consists of three mRNAs, $m1$, $m2$, and $m3$, which give rise to three proteins, $p1$, $p2$, and $p3$. Each protein inhibits the transcription of the next message (e.g. $p1$ represses $m2$). We varied the frequency of the oscillator by varying one of the translation rates by a factor ϕ. Oscillations were born and extinguished through supercritical Hopf bifurcations. The parameters for the model are as given by Elowitz and Leibler (*S4*).

ODEs:

$$\frac{dm_1}{dt} = -m_1 + \frac{\alpha}{1 + p_3^n} + \alpha_0$$

$$\frac{dm_2}{dt} = -m_2 + \frac{\alpha}{1 + p_1^n} + \alpha_0$$

$$\frac{dm_3}{dt} = -m_3 + \frac{\alpha}{1 + p_2^n} + \alpha_0$$

$$\frac{dp_1}{dt} = \beta\left(m_1 - \phi p_1\right)$$

$$\frac{dp_2}{dt} = \beta\left(m_2 - p_2\right)$$

$$\frac{dp_3}{dt} = \beta\left(m_3 - p_3\right)$$

Initial conditions:

$$m_1[0] = 1$$
$$m_2[0] = m_3[0] = p_1[0] = p_2[0] = p_3[0] = 0$$

Parameters:

$$n = 2$$
$$\alpha = 300$$
$$\alpha_0 = 0$$
$$\beta = 0.2$$

3. Pentilator. If the time scales of transcription and translation are separable, the Repressilator can be reduced to three ODEs. Since a two-ODE negative feedback loop cannot generate sustained oscillations, it seemed reasonable that a three ODE system would require careful balancing of kinetic parameters to oscillate, and would therefore oscillate over a limited range of frequencies. We were therefore curious to see if a five-ODE analog of the repressilator (the 'Pentilator') might have a qualitatively different amplitude/frequency relationship compared to the Repressilator and the other three ODE negative feedback oscillators being examined here. However, as shown in Figure 2, it turned out to behave very similarly to the Repressilator: oscillations were born and extinguished through supercritical Hopf bifurcations, and the operational frequency range of the model was small.

ODEs:

$$\frac{dm_1}{dt} = -m_1 + \frac{\alpha}{1 + p_5^n} + \alpha_0$$
$$\frac{dm_2}{dt} = -m_2 + \frac{\alpha}{1 + p_1^n} + \alpha_0$$
$$\frac{dm_3}{dt} = -m_3 + \frac{\alpha}{1 + p_2^n} + \alpha_0$$
$$\frac{dm_4}{dt} = -m_4 + \frac{\alpha}{1 + p_3^n} + \alpha_0$$
$$\frac{dm_5}{dt} = -m_5 + \frac{\alpha}{1 + p_4^n} + \alpha_0$$
$$\frac{dp_1}{dt} = \beta\left(m_1 - \phi p_1\right)$$
$$\frac{dp_2}{dt} = \beta\left(m_2 - p_2\right)$$

$$\frac{dp_3}{dt} = \beta(m_3 - p_3)$$

$$\frac{dp_4}{dt} = \beta(m_4 - p_4)$$

$$\frac{dp_5}{dt} = \beta(m_5 - p_5)$$

Initial conditions:

$$m_1[0] = 1$$
$$m_2[0] = m_3[0] = m_4[0] = m_5[0] = p_1[0] = p_2[0] = p_3[0] = p_4[0] = p_5[0] = 0$$

Parameters:

$$n = 2$$
$$\alpha = 300$$
$$\alpha_0 = 0$$
$$\beta = 0.2$$

4. Goodwin oscillator. The Goodwin model is a three-variable ODE system proposed forty years ago (*S5*), which has been applied to the analysis of circadian oscillations (*S6-S10*). The parameters used here were taken from Ruoff and co-workers (*S8*). Because they have emphasized that the frequency of the oscillator is a relatively sensitive function of the degradation rates, we chose the degradation rate constant to be the bifurcation parameter ϕ.

Note that for some of the parameter sets used by Ruoff and co-workers, the Goodwin model produces damped oscillations that approach a stable steady state (or stable spiral) rather than a stable limit cycle (*S8*). Here we examined only limit cycle oscillations.

ODEs:

$$\frac{dx}{dt} = \frac{k_1}{1 + z^9} - k_4 x$$

$$\frac{dy}{dt} = k_2 x - \phi y$$

$$\frac{dz}{dt} = k_3 y - k_6 z$$

Initial conditions:

$$x[0] = 0.0348$$
$$y[0] = 0.347$$
$$z[0] = 1.735$$

Parameters:

$$k_1 = 1$$
$$k_2 = 1$$
$$k_3 = 1$$
$$k_4 = 0.2$$
$$k_6 = 0.1$$

5. Frzilator. The Frzilator was proposed by Igoshin and co-workers to account for oscillatory swarming motions in *Myxococcus* (*S11*). The model consists of three ODEs and assumes that all of the activating and inactivating enzymes are highly saturated by their substrates. This model differs from the other negative feedback models considered here in that oscillations are born and extinguished through subcritical Hopf bifurcations rather than supercritical Hopf bifurcations. This means that there is a non-zero amplitude below which the model cannot generate sustained oscillations. It also means that near the bifurcations, a locally stable steady-state (or spiral) coexists with limit cycle oscillations, and the initial conditions determine which behavior is exhibited by the model.

ODEs:

$$\frac{df}{dt} = \phi\left(\frac{1-f}{0.01+(1-f)}\right) - d_f\left(\frac{f}{0.005+f}\right)e$$
$$\frac{dc}{dt} = k_c\left(\frac{1-c}{0.005+(1-c)}\right) - d_c\left(\frac{c}{0.005+c}\right)$$
$$\frac{de}{dt} = k_e\left(\frac{1-e}{0.005+(1-e)}\right) - d_e\left(\frac{e}{0.005+e}\right)$$

Initial conditions:

$$f[0] = 0.503$$
$$c[0] = 0.623$$
$$e[0] = 0.980$$

Parameters:

$k_c = 4$

$k_e = 4$

$d_f = 1$

$d_c = 2$

$d_e = 2$

6. Metabolator. The Metabolator is a synthetic gene-metabolic oscillator that rewires the glycolytic flux to drive an oscillation between two pools of metabolites in acetate pathway (*S12*). The design is based on two negative feedback loops. When acetyl phosphate (AcP) level increases, acetyl-CoA synthetase (Acs) is activated to drive the flux away from AcP, and phosphate acetyltransferase (Pta) is repressed to decrease the production of AcP. Here we vary the enzyme copy number ϕ in the model to change the frequency of the oscillations.

ODEs:

$$\frac{d[AcCoA]}{dt} = V_{Acs} - V_{pta} + V_{gly} - k_{TCA}[AcCoA]$$

$$\frac{d[AcP]}{dt} = V_{pta} - V_{Ack}$$

$$\frac{d[OAc^-]}{dt} = V_{Ack} - k_3[HOAc]$$

$$\frac{d[HOAc]}{dt} = V_{AcE} - k_3[HOAc]$$

$$\frac{d[lacI]}{dt} = \frac{\phi\left([AcP]/K_{g,1}\right)^n}{1+\left([AcP]/K_{g,1}\right)^n} + \alpha_0 - d[lacI]$$

$$\frac{d[Aca]}{dt} = \frac{a_1\phi\left([AcP]/K_{g,2}\right)^n}{1+\left([AcP]/K_{g,2}\right)^n} + a_1\alpha_0 - d[Acs]$$

$$\frac{d[pta]}{dt} = \frac{a_2\phi}{1+\left([lacI]/K_{g,3}\right)^n} + a_2\alpha_0 - d[pta]$$

where

$$V_{pta} = \frac{k_1[pta][AcCoA]}{K_{m1} + [AcCoA]}$$

$$V_{Acs} = \frac{k_2[Acs][OAc^-]}{K_{m2} + [OAc^-]}$$

$$V_{Ack} = k_{Ack,f}[AcP] - k_{Ack,r}[OAc^-]$$

$$V_{AcE} = 100\left([OAc^-][H^+] - K_{eq}[HOAc]\right)$$

$$V_{out} = k_3\left([HOAc] - [HOAc_E]\right)$$

Initial conditions:

$$AcCoA[0] = 0$$
$$AcP[0] = 2$$
$$OAc^-[0] = 0$$
$$HOAc[0] = 0.0009$$
$$lacI[0] = 0.00055$$
$$Acs[0] = 0.011$$
$$pta[0] = 0.00844$$

Parameters:

$$k_{TCA} = 10$$
$$k_1 = 80$$
$$k_2 = 0.8$$
$$K_{m1} = 0.06$$
$$K_{m2} = 0.1$$
$$k_{Ack,f} = k_{Ack,r} = 1$$
$$[H^+] = 10^{-7.6}$$
$$K_{eq} = 10^{-4.5}$$
$$k_3 = 0.01$$
$$a_0 = 0$$
$$a_1 = a_2 = 20$$
$$K_{g,1} = K_{g,2} = 10$$
$$K_{g,3} = 0.001$$
$$d = 0.06$$

The following four models are positive-plus-negative feedback oscillators:

7. Meyer and Stryer model of calcium oscillations. This is a three ODE model that accounts for many of the observed characteristics of cytosolic calcium oscillations (*S13*). The variable x represents cytoplasmic Ca^{2+}; y represents IP_3; and z represents ER Ca^{2+}. The parameter

R, which represents the fractional activation of a calcium-mobilizing G-protein coupled receptor, is used to vary the oscillator's frequency.

ODEs:

$$\frac{dx}{dt} = c_1 \frac{y^3}{(K_1 + y)^3} z - c_2 \frac{x^2}{(x + K_2)^2} + c_3 z^2 - c_6 (x / c_7)^{3.3} + c_6$$

$$\frac{dy}{dt} = c_4 R \frac{x}{x + K_3} - c_5 y$$

$$\frac{dz}{dt} = -c_1 \frac{y^3}{(K_1 + y)^3} z + c_2 \frac{x^2}{(x + K_2)^2} - c_3 z^2$$

Initial conditions:

$$x[0] = 0.1$$
$$y[0] = 0.01$$
$$z[0] = 25$$

Parameters:

$$c_1 = 6.64$$
$$c_2 = 5$$
$$c_3 = 0.0000313$$
$$c_4 = 1$$
$$c_5 = 2$$
$$c_6 = 0.5$$
$$c_7 = 0.6$$
$$K_1 = 0.1$$
$$K_2 = 0.15$$
$$K_3 = 1$$

8. van der Pol oscillator. The van der Pol oscillator model is a one-variable, second order differential equation, which can also be written as a pair of first order differential equations. The model has one parameter, ϕ, which was used to vary the frequency of oscillations.

ODEs:

$$\frac{dx}{dt} = y$$

$$\frac{dy}{dt} = \phi(1 - x^2) y - x$$

Initial conditions:

$$x[0] = 0.1$$
$$y[0] = 0$$

9. Fitzhugh-Nagumo oscillator. Parameters for the Fitzhugh-Nagumo relaxation oscillator (*S14, S15*) were taken from the Vibe website (*S16*). The coupling parameter ϕ was varied to change the frequency of the oscillations.

ODEs:

$$\frac{dv}{dt} = v(v-\theta)(1-v) - w + \omega$$
$$\frac{dw}{dt} = \phi(v - \gamma w)$$

Initial conditions:

$$v[0] = 0$$
$$w[0] = 0$$

Parameters:

$$\theta = 0.2$$
$$\omega = 0.112$$
$$\gamma = 2.5$$

10. Cyanobacteria circadian oscillator. The cyanobacterial circadian oscillator has been reconstituted in vitro using three purified proteins, KaiA, KaiB, and KaiC (*S17*). One of these proteins, KaiC, undergoes a sequence of phosphorylation and dephosphorylation reactions that produces the circadian cycles. Rust and co-workers have modeled these oscillations as a set of three experimentally-constrained ODEs that describe the interconversion of KaiC between a threonine-phosphorylated form (*T*), a doubly-phosphorylated form (*D*), and a serine-phosphorylated form (*S*) (*S18*). The remaining unphosphorylated form of KaiC can be calculated from these three forms and a conservation equation.

ODEs:

$$\frac{dT}{dt} = k_{UT}(S)U + k_{DT}(S)D - k_{TU}(S)T - k_{TD}(S)T$$
$$\frac{dD}{dt} = k_{TD}(S)T + k_{SD}(S)S - k_{DT}(S)D - k_{DS}(S)D$$

$$\frac{dS}{dt} = k_{US}(S)U + k_{DS}(S)D - k_{SU}(S)S - k_{SD}(S)S$$

where

$$k_{XY}(S) \equiv k_{XY}^{0} + \frac{k_{XY}^{A} A(S)}{K_{1/2} + A(S)}$$
$$A(S) \equiv \max\{0, [KaiA] - 2S\}$$

Initial conditions:

$$T[0] = 0.68$$
$$D[0] = 1.36$$
$$S[0] = 0.34$$

Parameters:

$$[KaiA] = 1.3$$
$$[KaiC]_{total} = U + T + D + S = 3.4$$
$$K_{1/2} = 0.43$$
$$k_{UT}^{0} = k_{TD}^{0} = k_{SD}^{0} = k_{US}^{0} = k_{DT}^{0} = 0$$
$$k_{TU}^{0} = 0.21$$
$$k_{DS}^{0} = 0.31$$
$$k_{SU}^{0} = 0.11$$
$$k_{UT}^{A} = 0.479$$
$$k_{TD}^{A} = 0.213$$
$$k_{SD}^{A} = 0.506$$
$$k_{US}^{A} = 0.053$$
$$k_{TU}^{A} = 0.0798$$
$$k_{DT}^{A} = 0.173$$
$$k_{DS}^{A} = \phi$$
$$k_{SU}^{A} = -0.133$$

Supplementary Figure S1:

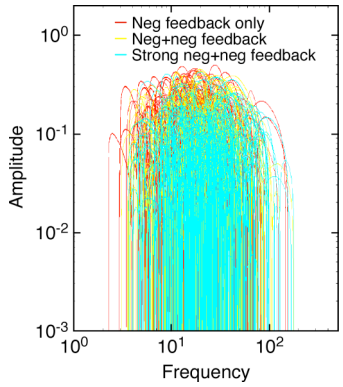

Fig. S1. Amplitude vs. frequency curves for randomly-parameterized oscillator models. Each curve corresponds to a different random parameter set. The red curves are from the negative-feedback-only model (Fig. 4A). The same curves are also included in Fig. 4F. The yellow and cyan curves are from the negative-plus-negative feedback model (Fig. 4C). The yellow curves correspond to weaker feedback (k_7=0-100) and the cyan curves to stronger feedback (k_7=500-600).

Table S1: Ranges for the random parameter sets

Parameter	Units	Range		Distribution
k_1	dimensionless	0 – 10		Uniform
k_2	dimensionless	0 – 1000		Uniform
k_3	dimensionless	0 – 10		Uniform
k_4	dimensionless	0 – 1000		Uniform
k_5	dimensionless	1		Fixed
k_6	dimensionless	0 – 1000		Uniform
k_7	dimensionless	Neg	0	Fixed
		Pos+neg, Neg+neg	0 – 100	Uniform
		Stronger pos+neg, Stronger neg+neg	500 – 600	Uniform
n_1	dimensionless	1 – 4		Uniform
n_2	dimensionless	1 – 4		Uniform
n_3	dimensionless	1 – 4		Uniform
n_4	dimensionless	1 – 4		Uniform
K_1	concentration	0 – 4		Uniform
K_2	concentration	0 – 4		Uniform
K_3	concentration	0 – 4		Uniform
K_4	concentration	0 – 4		Uniform

The parameters refer to the ordinary differential equation models shown in Figure 4A-C. The seven rate constants (k_1 through k_7) were non-dimensionalized by dividing by k_5.

References and Notes

S1. A. Dhooge, W. Govaerts, Y. A. Kuznetwov, *ACM Transactions on Mathematical Software* **29**, 141 (2003).
S2. J. R. Pomerening, S. Y. Kim, J. E. Ferrell, Jr., *Cell* **122**, 565 (2005).
S3. J. R. Pomerening, E. D. Sontag, J. E. Ferrell, Jr., *Nature Cell Biol*. **5**, 346 (2003).
S4. M. B. Elowitz, S. Leibler, *Nature* **403**, 335 (2000).
S5. B. C. Goodwin, Ed., *Oscillatory behavior in enzymatic control processes*, vol. 3 (Permagon Press, Oxford UK, 1965), vol. 3, pp. 425-438.
S6. P. Ruoff, S. Mohsenzadeh, L. Rensing, *Naturwissenschaften* **83**, 514 (1996).
S7. P. Ruoff, M. Vinsjevik, C. Monnerjahn, L. Rensing, *J. Theoret. Biol*. **209**, 29 (2001).
S8. P. Ruoff, M. Vinsjevik, C. Monnerjahn, L. Rensing, *J Biol. Rhythms* **14**, 469 (1999).
S9. P. Ruoff, M. Vinsjevik, S. Mohsenzadeh, L. Rensing, *J. Theoret. Biol*. **196**, 483 (1999).
S10. P. Ruoff, L. Rensing, R. Kommedal, S. Mohsenzadeh, *Chronobiol. Int*. **14**, 499 (1997).
S11. O. A. Igoshin, A. Goldbeter, D. Kaiser, G. Oster, *Proc. Natl. Acad. Sci. U.S.A*. **101**, 15760 (2004).
S12. E. Fung *et al*., *Nature* **435**, 118 (2005).
S13. T. Meyer, L. Stryer, *Proc. Natl. Acad. Sci. U.S.A*. **85**, 5051 (1988).
S14. R. FitzHugh, *Biophys. J*. **1**, 445 (1961).
S15. J. Nagumo, S. Arimoto, S. Yoshizawa, *Proc. IRE* **50**, 2061 (1964).
S16. D. S. Eck. *Vibe* (www.iro.umontreal.ca/~eckdoug/vibe/, 2003).
S17. M. Nakajima *et al*., *Science* **308**, 414 (2005).
S18. M. J. Rust, J. S. Markson, W. S. Lane, D. S. Fisher, E. K. O'Shea, *Science* **318**, 809 (2007).